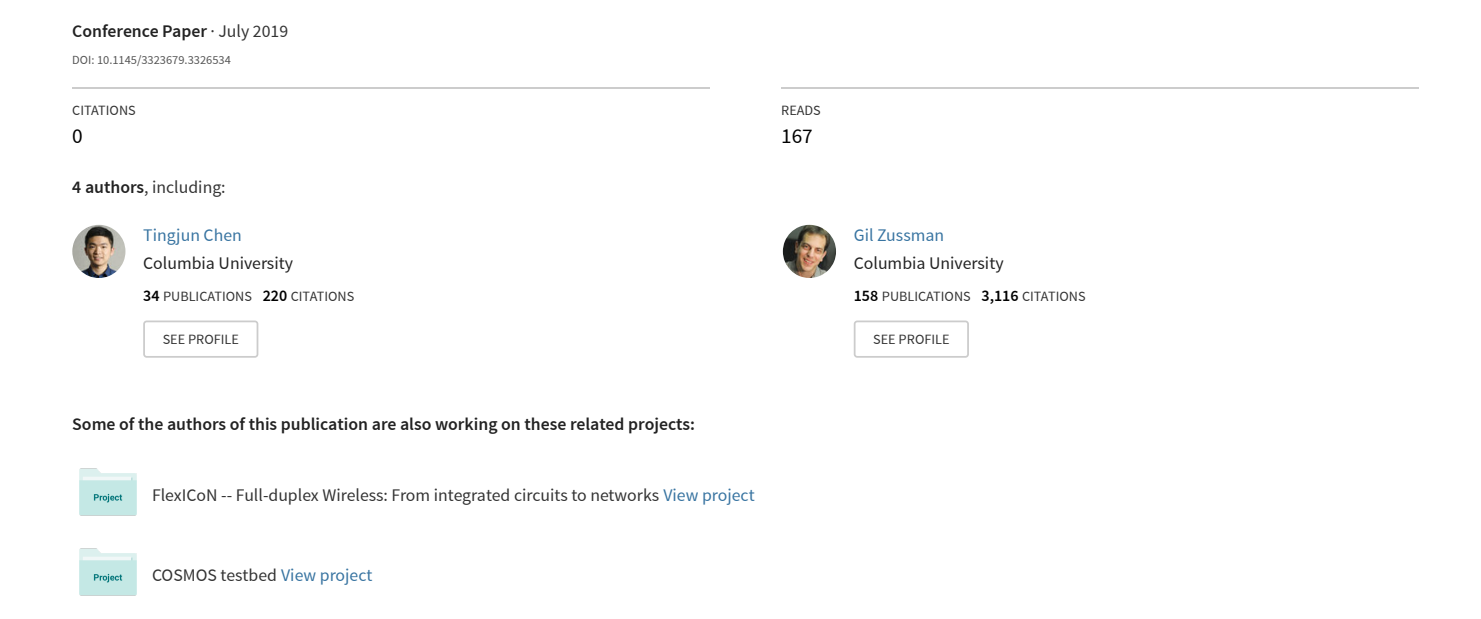
# Wideband Full-Duplex Phased Array with Joint Transmit and Receive Beamforming: Optimization and Rate Gains



# Wideband Full-Duplex Phased Array with Joint Transmit and Receive Beamforming: Optimization and Rate Gains

Tingjun Chen, Mahmood Baraani Dastjerdi, Harish Krishnaswamy, Gil Zussman
Electrical Engineering, Columbia University
{tingjun@ee., b.mahmood@, harish@ee., gil@ee.}columbia.edu

#### **ABSTRACT**

Full-duplex (FD) wireless and phased arrays are both promising techniques that can significantly improve data rates in future wireless networks. However, integrating FD with transmit (Tx) and receive (Rx) phased arrays is extremely challenging, due to the large number of self-interference (SI) channels. Previous work relies on either RF canceller hardware or on analog/digital Tx beamforming (TxBF) to achieve SI cancellation (SIC). However, Rx beamforming (RxBF) and the data rate gain introduced by FD nodes employing beamforming have not been considered yet. We study FD phased arrays with joint TxBF and RxBF with the objective of achieving improved FD data rates. The key idea is to carefully select the TxBF and RxBF weights to achieve wideband RF SIC in the spatial domain with minimal TxBF and RxBF gain losses. Essentially, TxBF and RxBF are repurposed, thereby not requiring specialized RF canceller circuitry. We formulate the corresponding optimization problem and develop an iterative algorithm to obtain an approximate solution with provable performance guarantees. Using SI channel measurements and datasets, we extensively evaluate the performance of the proposed approach in different use cases under various network settings. The results show that an FD phased array with 9/36/72 elements can cancel the total SI power to below the noise floor with sum TxBF and RxBF gain losses of 10.6/7.2/6.9 dB, even at Tx power level of 30 dBm. Moreover, the corresponding FD rate gains are at least  $1.33/1.66/1.68\times$ .

#### **CCS CONCEPTS**

• Networks  $\rightarrow$  Network architectures; Wireless access networks.

#### **KEYWORDS**

Full-duplex wireless; Phased array; Beamforming; Wideband selfinterference cancellation; Optimization

#### **ACM Reference Format:**

Tingjun Chen, Mahmood Baraani Dastjerdi, Harish Krishnaswamy, Gil Zussman. 2019. Wideband Full-Duplex Phased Array with Joint Transmit and Receive Beamforming: Optimization and Rate Gains. In Mobihoc '19: The Twentieth ACM International Symposium on Mobile Ad Hoc Networking and Computing, July 2–5, 2019, Catania, Italy. ACM, New York, NY, USA, 10 pages. https://doi.org/10.1145/3323679.3326534

Permission to make digital or hard copies of all or part of this work for personal or classroom use is granted without fee provided that copies are not made or distributed for profit or commercial advantage and that copies bear this notice and the full citation on the first page. Copyrights for components of this work owned by others than ACM must be honored. Abstracting with credit is permitted. To copy otherwise, or republish, to post on servers or to redistribute to lists, requires prior specific permission and/or a fee. Request permissions from permissions@acm.org.

Mobihoc '19, July 2–5, 2019, Catania, Italy © 2019 Association for Computing Machinery. ACM ISBN 978-1-4503-6764-6/19/07...\$15.00 https://doi.org/10.1145/3323679.3326534

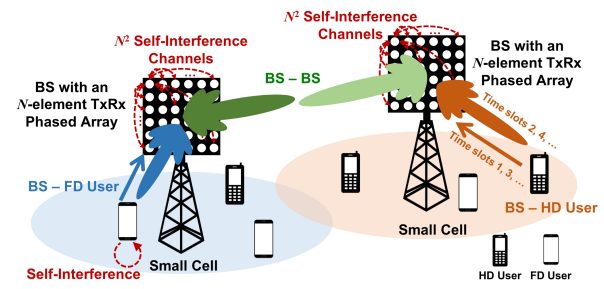


Figure 1: Example network scenarios where a base station (BS) is equipped with an N-element TxRx phased array employing transmit and receive beamforming. Considered use cases: (i) BS-User: uplink-downlink (UL-DL) transmission between the BS and a user in HD (orange) or FD (blue) mode, and (ii) BS-BS: bidirectional transmission between two BSs in HD (beamforming in dark/light green in alternate time slots) or FD (simultaneous beamforming in dark/light green) mode.

#### 1 INTRODUCTION

Full-duplex (FD) wireless – simultaneous transmission and reception on the same frequency – has the potential to double the throughput and reduce latency, thereby has attracted significant attention [17, 22]. The fundamental challenge associated with FD wireless is the vast amount of self-interference (SI) leaking from the transmitter (Tx) into the receiver (Rx), which needs to be canceled to successfully recover the desired signal. Recent work has demonstrated practical levels of SI cancellation (SIC) at the antenna interface, RF/analog, and digital baseband [6, 9, 11, 14, 28].

Another important technology is Tx (resp. Rx) phased arrays which can substantially enhance the communication range through analog Tx beamforming (TxBF) (resp. Rx beamforming (RxBF)), a technique for directional signal transmission (resp. reception) utilizing spatial selectivity [12, 25]. TxBF/RxBF can provide significantly increased Tx/Rx signal power at the same link distance, or enhanced link distance at the same signal-to-noise ratio (SNR).

Although combining FD with phased arrays can provide significantly improved data rates, it poses numerous challenges. First, in an N-element FD phased array (see Fig. 1),  $N^2$  SI channels between every pair of Tx and Rx elements need to be canceled in the RF domain. Techniques using circuits (e.g., [5]) or alternating antenna placements (e.g., [3]) to achieve wideband RF SIC do not directly apply to an FD phased array. This is because that RF cancellers are expensive while the cancellation via antenna placements usually requires at least twice the antennas. Accordingly, both techniques cannot scale to large phased arrays. Moreover, although the conventional half-duplex (HD) TxBF and RxBF can each provide a maximum beamforming gain of N [12], the total SI power can also potentially add up constructively by a factor of  $N^2$ . Therefore, innovative solutions are needed to achieve FD operation in phased arrays.

In this paper, we show that by carefully selecting the Tx and Rx analog beamforming weights (a.k.a., beamformers), an FD phased array can simultaneously achieve wideband RF SIC with minimal TxBF and RxBF gain losses, and improved FD rate gains. In other words, TxBF and RxBF can be repurposed to support wideband RF SIC. A key insight of our approach is that in multi-antenna systems, the spatial domain (i.e., across Tx and Rx elements) represents another dimension in which RF SIC can be achieved. The advantage of this approach is manifold: the RF SIC based on joint TxBF and RxBF (i) is wideband since the SI channels between every pair of Tx and Rx elements experience similar delays, (ii) does not require specialized RF SIC circuitry, thus reducing the total power consumption, (iii) is achieved before the digital domain, which largely reduces the analog-to-digital converter (ADC) dynamic range and power consumption, and (iv) will benefit from large-scale antenna arrays where a large number of TxBF and RxBF weights can be modified.

We consider network scenarios as depicted in Fig. 1, where a BS is an *N*-element FD phased array (see Fig. 3(a)). We consider two use cases where an FD BS communicates with: (i) a single-antenna user which is HD- or FD-capable (the *BS-User* case), or (ii) with another FD BS (the *BS-BS* case), and derive the data rate gain resulting from using FD. Specifically, the FD link objective is to *maximize the FD data rate gains* by optimizing the FD Tx and Rx beamformers with minimal TxBF and RxBF gain losses. We demonstrate the FD rate gains introduced by FD phased arrays employing TxBF and RxBF in various network settings with different Tx power levels and link SNR values. Based on the Argos FD channel measurements [1, 23], we show that in the BS-User case, a 36-element FD phased array with Tx power of 20 dBm can achieve maximum FD rate gains of 1.27/1.60/1.72× with 0/15/30 dB link SNR values, and with TxBF and RxBF gain losses of only 3.1 dB.

Based on the FD link objective, we formulate an optimization problem to jointly determine the optimal FD Tx and Rx beamformers. Due to its non-convexity and analytical intractability, we then present alternative convex optimization problems by leveraging the structural properties of the SI channel matrix and its coupling with the Tx and Rx beamformers. We develop an iterative algorithm that efficiently solves the alternative optimization problems with provable performance guarantees.

We numerically evaluate the network performance and the corresponding FD rate gains when using the iterative algorithm, based on SI channel measurements and datasets. Extensive evaluations are conducted under different network scenarios and a wide range of number of antennas, antenna array geometries, and Tx power levels. Specifically, the results show that an FD phased array with 9/36/72 elements can cancel the total SI power to below the noise floor with sum TxBF and RxBF gain losses of 10.6/7.2/6.9 dB, even at Tx power level of 30 dBm (note that the conventional HD TxBF and RxBF can provide sum TxBF and RxBF gains of 19.1/30.1/37.1 dB). Moreover, the *FD rate gains* in the BS-User case are at least 1.33/1.66/1.68× with N=9/36/72. The FD rate gains in the BS-BS case are at least 1.53× with  $N\geq 36$  in all considered SNR regimes.

To summarize, the main contributions of this paper are: (i) an FD phased array model that employs joint TxBF and RxBF for simultaneously achieving high FD rate gains and wideband RF SIC, (ii) an efficient iterative algorithm for obtaining the FD Tx and

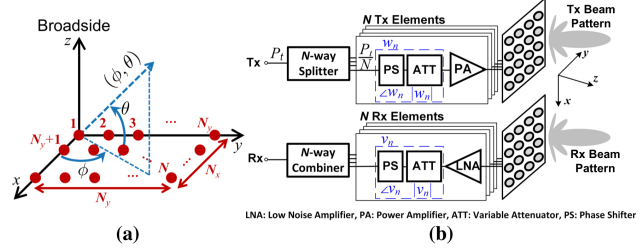


Figure 2: (a) An example N-element rectangular antenna array in a spherical coordinate system, (b) block diagrams of N-element Tx (top) and Rx (bottom) phased arrays in the HD setting.

Rx beamformers with provable performance guarantees, and (iii) extensive performance evaluation of the proposed approach.

#### 2 RELATED WORK

Recent work focused on the design and implementation of FD radios and systems, either using off-the-shelf components [6, 14] or based on integrated circuits (ICs) [9, 17, 28] (see the review in [22] and references therein). For single-antenna FD, a pair of Tx and Rx antennas with proper separation, or a shared antenna interface using a circulator, have been used. In this case, RF SIC is achieved by an *additional* cancellation circuitry. FD MIMO radio implementations have been presented in [3, 5], where up to 3 Tx/Rx antennas are considered and RF SIC is achieved using either RF cancellers or through alternating antenna placements.

At the higher layers, FD rate gain with single-antenna FD radios has been studied analytically at the link-level [19], and experimentally at the link- and network-level [9]. Recent work also explores medium access control and scheduling in FD networks [10, 15, 20] as well as FD relays [7, 21, 26]. FD also facilitates different applications including neighbor discovery [24] and localization [18].

Most relevant to our work are [2, 16]. In particular, [16] considers an FD multi-user MIMO downlink channel with *separate* Tx and Rx antennas and applies *digital* TxBF to achieve RF SIC. This differs from our approach, which is based on joint analog TxBF and RxBF and results in lower power consumption. On the other hand, in [2], *narrowband* RF SIC is achieved via *only* analog TxBF for phased arrays with separate Tx and Rx antennas. Moreover, our previous work [13] focuses on IC implementations of an FD phased array with only 8 elements. However, the optimization of the TxBF and RxBF, and the FD link rate gains in different network scenarios have not be addressed. To the best of our knowledge, this is *the first fundamental study of these topics*.

#### 3 BACKGROUND ON PHASED ARRAYS

In this section, we follow [12] and provide background on phased arrays and beamforming in the half-duplex setting. Beamforming is a technique that uses an antenna phased array to achieve directional signal transmission or reception. For completeness, we describe Tx and Rx phased arrays, and Tx and Rx beamforming (TxBF and RxBF). We provide an overview of the steering vector and Tx/Rx arrays, followed by the important characteristics of beamforming including array factor, beam pattern, and beamforming gain.

**Steering Vector**. Denote by N the number of antennas in the array (see Fig. 2(a)). A spherical coordinate system is considered where the azimuth and elevation angles are denoted by  $\phi$  and  $\theta$ , respectively.

Let  $s_n(\phi,\theta)$  be the relevant phase delay experienced by a plane wave as it departs/reaches the  $n^{\text{th}}$  Tx/Rx element in the spatial direction of  $(\phi,\theta)$ . Consider an example N-element rectangular antenna array with  $N_x$  rows and  $N_y$  columns  $(N_x \cdot N_y = N)$ , where the antennas are indexed as shown in Fig. 2(a). Assuming half-wavelength spacing between adjacent antennas,  $s_n(\phi,\theta)$  for the  $n^{\text{th}}$  element at location  $(n_x,n_y)$ , where  $n=(n_x-1)N_y+n_y$ , is

$$s_n(\phi,\theta) = e^{j\pi[(n_x-1)\cos\theta\cos\phi + (n_y-1)\cos\theta\sin\phi]}, \forall n_x, n_y.$$

The *steering vector* in the direction of  $(\phi, \theta)$  is then given by  $\mathbf{s}(\phi, \theta) = [s_n(\phi, \theta)] \in \mathbb{C}^N$ , which depends on the antenna array geometry. **Transmit (Tx) and Receive (Rx) Arrays, and Analog Beamformer**. As illustrated in Fig. 2(b), in an N element Tv erroy with

**former**. As illustrated in Fig. 2(b), in an N-element Tx array with total Tx power of  $P_t$ , each Tx element consists of a power amplifier (PA), a variable attenuator (ATT), and a phase shifter (PS). Symmetrically, in an N-element Rx array, each Rx element consists of a lower noise amplifier (LNA), a variable attenuator, and a phase shifter. Denote by  $P_{\rm nf}$  the noise floor of a single Rx element. Then, the Rx array has an array noise floor of  $N \cdot P_{\rm nf}$  due to the aggregated noise from all Rx elements. We assume the followings: (i) with an ideal power splitter, each Tx element has a maximum Tx power of  $P_t/N$ , and (ii) the LNA of each Rx element has a unit gain of 1.

An analog beamformer is the set of complex-valued weights applied to each element relative to that of the first element. Specifically, denote the weight applied to the  $n^{\text{th}}$  Tx (resp. Rx) element by  $w_n = |w_n| \cdot e^{j \angle w_n}$  (resp.  $v_n = |v_n| \cdot e^{j \angle v_n}$ ) with amplitude  $|w_n|$  (resp.  $|v_n|$ ) and phase  $\angle w_n$  (resp.  $\angle v_n$ ). In particular,  $|w_n|^2$ ,  $|v_n|^2 \le 1$  represent the variable gain on the  $n^{\text{th}}$  Tx/Rx element controlled by the attenuator.  $\angle w_n$ ,  $\angle v_n \in [-\pi, \pi]$  represent the phase on the  $n^{\text{th}}$  Tx/Rx element controlled by the phase shifter. The vectors  $\mathbf{w} = [w_n] \in \mathbb{C}^N$  and  $\mathbf{v} = [v_n] \in \mathbb{C}^N$  are called the Tx and Tx (analog) beamformers, respectively.

Array Factor, Beam Pattern, and Beamforming Gain. An analog beamformer features (N-1) degrees of freedom (DoF), which are typically configured to alter the *beam pattern* (see Fig. 2(b)) to enhance the signal directivity and/or to suppress interference by constructing nulls. The far-field Tx and Rx *array factors* in the direction of  $(\phi, \theta)$ , which quantify the effect of combining weighted transmitting Tx and receiving Rx elements, are given by [12]

$$A_{\mathbf{t}}(\phi, \theta) = \mathbf{s}^{\mathsf{T}}(\phi, \theta) \cdot \mathbf{w} \in \mathbb{C}, \ A_{\mathbf{r}}(\phi, \theta) = \mathbf{s}^{\mathsf{T}}(\phi, \theta) \cdot \mathbf{v} \in \mathbb{C}.$$

The corresponding far-field Tx and Rx beam patterns are defined as

$$\begin{cases} E_{\mathbf{t}}(\phi, \theta) = |A_{\mathbf{t}}(\phi, \theta)|^2 = |\mathbf{s}^{\top}(\phi, \theta) \cdot \mathbf{w}|^2, \\ E_{\mathbf{r}}(\phi, \theta) = |A_{\mathbf{r}}(\phi, \theta)|^2 = |\mathbf{s}^{\top}(\phi, \theta) \cdot \mathbf{v}|^2. \end{cases}$$
(1)

The Tx beamforming (TxBF) gain (resp. Rx beamforming (RxBF) gain) is defined as the power gain of the Tx (resp. Rx) signal in the far-field normalized to the maximum total Tx (resp. Rx) power. Denote by  $G_t(\phi,\theta)$  and  $G_r(\phi,\theta)$ ) the TxBF gain and RxBF gain in the spatial direction of  $(\phi,\theta)$ , respectively. They are given by

$$\begin{cases} G_{t}(\phi, \theta) = E_{t}(\phi, \theta)/N = |\mathbf{s}^{\top}(\phi, \theta) \cdot \mathbf{w}|^{2}/N, \\ G_{r}(\phi, \theta) = E_{r}(\phi, \theta)/N = |\mathbf{s}^{\top}(\phi, \theta) \cdot \mathbf{v}|^{2}/N. \end{cases}$$
(2)

Denote the *desired* Tx and Rx beam-pointing directions by  $(\phi_t, \theta_t)$  and  $(\phi_r, \theta_r)$ . Let  $s_t$  and  $s_r$  be the steering vectors in the desired Tx and Rx beam-pointing directions, i.e.,  $s_t = s(\phi_t, \theta_t)$ ,  $s_r = s(\phi_r, \theta_r)$ . The (complex-valued) Tx and Rx array factors in the desired beam-pointing directions, denoted by  $a_t$  and  $a_r$ , are then given by

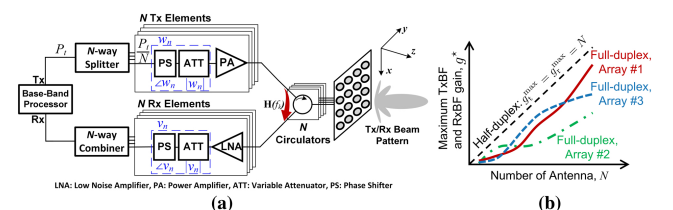


Figure 3: (a) Block diagram of an N-element FD phased array with SI channel matrix,  $H(f_k)$ , where a Tx and an Rx phased arrays are connected to the antennas through circulators, (b) illustration of the relationship between the maximum TxBF and RxBF gains,  $g_t^{\star} = g_r^{\star} = g^{\star}$ , that can be achieved by an FD phased array after repurposing TxBF and RxBF for wideband RF SIC, and the number of antennas, N, for various array geometries.

$$a_t = A_t(\phi_t, \theta_t) = \mathbf{s}_t^\top \mathbf{w}, \ a_r = A_r(\phi_r, \theta_r) = \mathbf{s}_r^\top \mathbf{v}.$$
 (3)

Therefore, the TxBF and RxBF gains in the desired Tx and Rx beampointing directions, denoted by  $g_{\rm t}$  and  $g_{\rm r}$ , are given by

$$g_t = |a_t|^2 / N, \ g_r = |a_r|^2 / N.$$
 (4)

Note that since  $g_t$  and  $g_r$  are the normalized power gains introduced by TxBF and RxBF, respectively, they *do not* depend on the absolute power levels of the Tx and Rx signals.

**Conventional (Half-Duplex) TxBF and RxBF.** It is known that by setting  $\mathbf{w} = \mathbf{s}_{t}^{*}$  (resp.  $\mathbf{v} = \mathbf{s}_{r}^{*}$ ), a maximum Tx (resp. Rx) array factor of N and a maximum TxBF (resp. RxBF) gain of N in the desired beam-pointing direction can be achieved [12], i.e.,

$$a_{\rm t}^{\rm max}={\bf s}_{\rm t}^{\rm T}{\bf s}_{\rm t}^*=N,\ a_{\rm r}^{\rm max}={\bf s}_{\rm r}^{\rm T}{\bf s}_{\rm r}^*=N,\ {\rm and}\ g_{\rm t}^{\rm max}=g_{\rm r}^{\rm max}=N.$$
 (5) Accordingly, we refer to  ${\bf w}_{\rm conv}={\bf s}_{\rm t}^*$  and  ${\bf v}_{\rm conv}={\bf s}_{\rm r}^*$  as the *conventional HD Tx and Rx beamformers*, respectively.

# 4 MODEL, RATES, AND OBJECTIVE

We present the model of an FD phased array node combining TxBF and RxBF and the corresponding FD TxBF and RxBF gains. Then, we discuss the data rate gains obtained by FD and the FD link objective.

#### 4.1 FD Phased Array Model

We consider an FD phased array node as depicted in Fig. 3(a). A BS is equipped with an N-element FD phased array, where each antenna is shared between a pair of Tx and Rx elements via a circulator, and where TxBF and RxBF are applied. As shown in Fig. 1, a user has a single antenna and does not apply beamforming. We use b and u in the subscript to denote the BS and user. Consider a wireless bandwidth of B that is divided into K orthogonal frequency channels. The channels are indexed by  $k \in \{1, \ldots, K\}$  and the kth channel's center frequency is  $f_k$ . Without loss of generality, we assume an OFDM-based system with bandwidth B and K subcarriers.

**SI Channel Matrix**. Similar to [16], we let  $H_{nn}(f_k)$ ,  $\forall n$ , denote the frequency response of the SI channel from the  $n^{\text{th}}$  Tx element to the  $n^{\text{th}}$  Rx element at frequency  $f_k$ ,  $\forall k$ , and let  $H_{mn}(f_k)$ ,  $\forall m \neq n$ , denote the frequency response of the cross-talk SI (CTSI) channel from the  $n^{\text{th}}$  Tx element to the  $m^{\text{th}}$  Rx element at frequency  $f_k$ ,  $\forall k$ . We then denote  $H(f_k) = [H_{mn}(f_k)] \in \mathbb{C}^{N \times N}$  as the SI channel matrix of the TxRx array at frequency  $f_k$ ,  $\forall k$ , consisting of all the  $N^2$  SI and CTSI channels, as shown in Fig 1. We assume  $|H_{mn}(f_k)| \leq 1$ ,  $\forall i, j, k$ , due to the propagation loss of the Tx signal. Ideally, due to channel reciprocity,  $H_{mn}(f_k) = H_{nm}(f_k)$ ,  $\forall k$ , for any Tx and Rx element pair (n, m), resulting in  $H(f_k) = H^T(f_k)$ .

However, as we will show in Section 7.1, this does not hold in a realistic environment, due to effects such as imperfections of antenna matching and environmental interference and noise.1

**Use Cases**. We consider four use cases as depicted in Fig. 1:

- (i) BS-User (HD or FD): uplink-downlink (UL-DL) transmission between a BS and a user in HD (orange) or FD (blue) mode,
- (ii) BS-BS (HD or FD): bidirectional transmission between two BSs in HD (beamforming in dark/light green in alternate time slots) or FD (simultaneous beamforming in dark/light green) mode.

The cases where the BSs or the user operate in HD mode and the channel is shared in a TDD manner are considered as the benchmark HD cases. When operating in FD mode, a BS applies simultaneous TxBF and RxBF when communicating with an FD user or another FD BS. We also assume that the BS has the information regarding the direction of an intended user or another BS.

Self-Interference-to-Noise Ratio (XINR) under TxBF and RxBF. For an FD node, XINR is defined as the ratio between the residual SI power after analog and digital SIC and the noise floor. Let  $\gamma_{hh}(f_k)$ and  $\gamma_{uu}(f_k)$  denote the XINR of the BS and the user at frequency  $f_k$ , respectively, when operating in FD mode. Since our focus is on the SIC at the BS with TxBF and RxBF, we assume that a user can always cancel its SI to below the noise floor, i.e.,  $\gamma_{uu}(f_k) \le 1, \forall k \ [9, 28]$ . Accordingly, a user transmits at the maximum possible power level when operating in either HD or FD mode.

For the BS, denote by  $P_{SI}^{bf}(f_k)$  the SI power under TxBF and RxBF, and by  $SIC_{
m dig}$  the amount of achievable digital SIC.  $^2$  Recall that the BS has an Rx array noise floor of  $NP_{\rm nf}$ , the XINR at  $f_k$  is given by

$$\gamma_{bb}(f_k) = \frac{P_{\rm SI}^{\rm bf}(f_k)}{SIC_{\rm dig} \cdot (NP_{\rm nf})}, \ \forall k.$$
 (6)

We now derive  $\gamma_{hh}(f_k)$  under TxBF and RxBF. Without loss of generality, we assume a wideband (e.g., OFDM) transmit symbol  $x(f_k) \in \mathbb{C}$  with unit power of  $|x(f_k)|^2 = 1, \forall k$ . The received SI symbol, denoted by  $y(f_k) \in \mathbb{C}$ , is given by

$$y(f_k) = \sum_{m=1}^{N} \sum_{n=1}^{N} \left[ w_n \cdot H_{mn}(f_k) \cdot v_m \right] \cdot \sqrt{\frac{P_t}{N}} \cdot x(f_k) + z$$
$$= \sqrt{\frac{P_t}{N}} \cdot \mathbf{v}^\top \mathbf{H}(f_k) \mathbf{w} \cdot x(f_k) + z, \ \forall k,$$

where z is the additive white Gaussian noise. Then, the SI power is

$$P_{\mathrm{SI}}^{\mathrm{bf}}(f_k) = |y(f_k)|^2 = |\mathbf{v}^{\mathsf{T}}\mathbf{H}(f_k)\mathbf{w}|^2 \cdot \frac{P_{\mathrm{t}}}{N}, \ \forall k. \tag{7}$$

$$P_{SI}^{bf}(f_k) = |y(f_k)|^2 = |\mathbf{v}^{\mathsf{T}}\mathbf{H}(f_k)\mathbf{w}|^2 \cdot \frac{P_{\mathsf{t}}}{N}, \ \forall k.$$
(7)  
Plugging (7) into (6) yields the XINR of the BS:  
$$\gamma_{bb}(f_k) = \frac{|y(f_k)|^2}{SIC_{\mathsf{dig}} \cdot (NP_{\mathsf{nf}})} = \frac{|\mathbf{v}^{\mathsf{T}}\mathbf{H}(f_k)\mathbf{w}|^2}{SIC_{\mathsf{dig}}NP_{\mathsf{nf}}} \cdot \frac{P_{\mathsf{t}}}{N}, \ \forall k.$$
(8)

#### FD Beamformers and Beamforming Gains

A maximum TxBF and RxBF gain of *N* can be achieved under the conventional HD Tx and Rx beamformers,  $\mathbf{w}_{conv}$  and  $\mathbf{v}_{conv}$  (see (5)). However, as we will show in Section 7.3, the XINR under  $\mathbf{w}_{conv}$  and  $\mathbf{v}_{\text{conv}}$  is significant, i.e.,  $\gamma_{bb}(f_k) \gg 1, \forall k$ . Therefore, using these beamforming weights is impractical for a BS operating in FD mode.

To support FD operation, we aim to achieve wideband RF SIC in an FD phased array only through manipulating the TxBF and RxBF weights, w and v, thereby not requiring specific RF canceller hardware or circuitry (see Section 1). Specifically, we aim to achieve both  $\gamma_{hh}(f_k) \leq 1, \forall k$ , and the maximum FD data rate gain by properly selecting w and v. However, these weights, termed as the FD Tx and Rx beamformers, may not achieve the maximum TxBF and RxBF gain of N as in the conventional HD setting. Accordingly, we define the optimal FD TxBF and RxBF gain as follows.

DEFINITION 4.1 (OPTIMAL FD TXBF AND RXBF GAIN). For a given FD phased array with  $H(f_k)$  and  $P_t$ , the optimal FD TxBF and RxBF gain is the equal maximum TxBF and RxBF gains that can be achieved while satisfying  $\gamma_{hh}(f_k) \leq 1, \forall k$ .

Denote by  $g_{\rm t}^{\star}=g_{\rm r}^{\star}=g^{\star}$  the optimal FD TxBF and RxBF gain, and by  $a_{\rm f}^{\star}$  and  $a_{\rm r}^{\star}$  the corresponding optimal FD Tx and Rx array factors (the reason for setting  $g_t^{\star} = g_r^{\star}$  is described in Section 4.4). From (4),  $g_t^{\star} = |a_t^{\star}|^2/N$  and  $g_r^{\star} = |a_r^{\star}|^2/N$ . To quantify the performance of FD TxBF and RxBF, we present the following definition.

DEFINITION 4.2 (TxBF AND RxBF GAIN Losses). The TxBF gain loss is the ratio between the maximum HD TxBF gain and the optimal FD TxBF gain, i.e.,  $\frac{N}{q_{\star}^{*}}$ . Symmetrically, the RxBF gain loss is  $\frac{N}{q_{\star}^{*}}$ .

The TxBF and RxBF gain losses are typically represented in dB. For example, a 3 dB TxBF gain loss means that the far-field Tx power is reduced by half, since  $g_t^{\star} = 0.5N \Rightarrow 10 \log_{10}(N/g_t^{\star}) = 3 \text{ dB}$ . Similarly, a 6 dB TxBF gain loss corresponds to  $g_t^* = 0.25N$ .

Fig. 3(b) pictorially illustrates the relationship between  $g^*$  and the number of antennas, N, for various array geometries, where different antenna arrays may have different  $q^*$ . In particular, for a given FD phased array with  $H(f_k)$  and Tx power level  $P_t$ , there exists a pair of optimal FD Tx and Rx beamformers that achieves  $g^*$  while satisfying  $\gamma_{bb}(f_k) \leq 1, \forall k$ . The FD phased array will experience higher TxBF and RxBF gains with increased value of N, since a larger number of Tx and Rx weights can be manipulated.

#### Sum Link Rate and FD Rate Gain

We now derive the HD and FD data rates and the effect of the optimal FD TxBF and RxBF gain on the FD rates. Denote by y the link SNR without beamforming. We use Shannon's capacity formula to compute the rate on a link with bandwidth, B, and link SNR, y. Since the TxBF and RxBF gains,  $g_t$  and  $g_r$ , are independent of the absolute power of the Tx and Rx signals (see Section 3), the link SNR improvement introduced by beamforming equals to  $q_t$  and  $q_r$ in the desired Tx and Rx beam-pointing directions, respectively.

For the BS-User case, we denote by  $\gamma_{bu}$  ( $u \rightarrow b$ ) and  $\gamma_{ub}$  ( $b \rightarrow u$ ) the UL and DL SNRs, respectively. For the BS-BS case, we index the BSs by  $b_1$  and  $b_2$  and denote the link SNRs by  $\gamma_{b_1b_2}$   $(b_2 \rightarrow b_1)$ and  $\gamma_{b_2b_1}$  ( $b_1 \rightarrow b_2$ ). The sum of the HD link rates in both cases, when the BSs and user operate in HD mode and share the channel in a TDD manner equally (i.e., each link is activated for 50% of the time), are given by

$$r_{\text{BS-User}}^{\text{HD}} = \frac{B}{2} \log_2 (1 + N\gamma_{bu}) + \frac{B}{2} \log_2 (1 + N\gamma_{ub}),$$
 (9)

 $r_{\text{RS-BS}}^{\text{HD}} = \tfrac{B}{2} \log_2 \left( 1 + N^2 \gamma_{b_1 b_2} \right) + \tfrac{B}{2} \log_2 \left( 1 + N^2 \gamma_{b_2 b_1} \right).$ (10)In particular, the UL and DL SNR improvements in the BS-User case (9) result from the maximum RxBF and TxBF gains of N in the desired beam-pointing directions. Similarly, the SNR improvements in the BS-BS case (10), which are factors of  $g_t^{\text{max}} g_r^{\text{max}} = N^2$  for both  $\gamma_{b_1b_2}$  and  $\gamma_{b_2b_1}$ , stem from the combined TxBF and RxBF gains of both BSs in the desired beam-pointing directions.

<sup>&</sup>lt;sup>1</sup>Note that our model and results also apply to an FD phased array where the Tx and Rx arrays are equipped with seperate antennas, which requires twice many antenna elements (as illustrated in Fig. 3(a)). Such separated Tx and Rx antennas usually provide better isolation (i.e., smaller values of  $|H_{mn}(f_k)|$ ) than a shared antenna interface. <sup>2</sup>We assume that SIC<sub>dig</sub> is constant across frequency, since delay taps can be easily generated in the digital domain [6].

When the BSs and user operate in FD mode, the link SNRs are affected by both the degraded TxBF and RxBF gains,  $g_{\rm t}^{\star}$  and  $g_{\rm r}^{\star}$ , and the frequency-dependent XINR of the BS and user,  $\gamma_{bb}(f_k)$  and  $\gamma_{uu}(f_k)$ , respectively. As a result, the sum of the FD link rates in both use cases are given by

$$r_{\text{BS-User}}^{\text{FD}} = \frac{B}{K} \sum_{k=1}^{K} \log_2 \left( 1 + \frac{g_t^{\star} \gamma_{bu}}{1 + \gamma_{bb}(f_k)} \right) + \log_2 \left( 1 + \frac{g_t^{\star} \gamma_{ub}}{1 + \gamma_{uu}(f_k)} \right), \quad (11)$$

$$r_{\text{BS-BS}}^{\text{FD}} = \frac{B}{K} \sum_{k=1}^{K} \log_2 \left( 1 + \frac{g_t^{\star} g_r^{\star} \gamma_{b_1 b_2}}{1 + \gamma_{bb}(f_k)} \right) + \log_2 \left( 1 + \frac{g_t^{\star} g_r^{\star} \gamma_{b_2 b_1}}{1 + \gamma_{bb}(f_k)} \right). \quad (12)$$

Due to the coupling between  $g_t^{\star}$ ,  $g_r^{\star}$ , and  $\gamma_{bb}(f_k)$  through the Tx and Rx beamformers, **w** and **v** (see (8)), and the frequency-dependent  $H(f_k)$ , maximizing (11) and (12) presents numerous challenges. To allow analytical tractability, we approximate the FD sum rates in (11) and (12) by setting  $\gamma_{uu}(f_k) = \gamma_{bb}(f_k) = 1$ ,  $\forall k$ . We refer to the approximated FD sum rates as  $\widetilde{r}_{BS-User}^{FD}$  and  $\widetilde{r}_{BS-BS}^{FD}$ , respectively, and they are given by

$$\widetilde{r}_{\text{BS-User}}^{\text{FD}} = B \left[ \log_2 \left( 1 + \frac{g_{\scriptscriptstyle \text{I}}^{\star} \gamma_{bu}}{2} \right) + \log_2 \left( 1 + \frac{g_{\scriptscriptstyle \text{I}}^{\star} \gamma_{ub}}{2} \right) \right], \tag{13}$$

$$\widetilde{r}_{\text{BS-User}}^{\text{FD}} = B \Big[ \log_2 \Big( 1 + \frac{g_1^\star g_1^\star \gamma_{b_1 b_2}}{2} \Big) + \log_2 \Big( 1 + \frac{g_1^\star g_1^\star \gamma_{b_2 b_1}}{2} \Big) \Big].$$
 (14) Recall that  $\gamma_{uu}(f_k) \leq 1$  and we aim to achieve  $\gamma_{bb}(f_k) \leq 1$  (0 dB) for an FD phased array. Therefore,  $\widetilde{r}_{\text{BS-User}}^{\text{FD}}$  and  $\widetilde{r}_{\text{BS-BS}}^{\text{FD}}$  are lower bounds of the FD sum rates,  $r_{\text{BS-User}}^{\text{FD}}$  and  $r_{\text{BS-BS}}^{\text{FD}}$ , given in (11)–(12). In the rest of the paper, we focus on maximizing  $\widetilde{r}_{\text{BS-User}}^{\text{FD}}$  and  $\widetilde{r}_{\text{BS-User}}^{\text{FD}}$ .

In the rest of the paper, we focus on maximizing  $\tilde{r}_{\text{BS-User}}^{\text{FD}}$  and  $\tilde{r}_{\text{BS-BS}}^{\text{FD}}$ . We define the *FD rate gain* in the BS-User (resp. BS-BS) case as the ratio between the FD sum rate lower bound and the HD sum rate, i.e.,  $\tilde{r}_{\text{BS-User}}^{\text{FD}}/r_{\text{BS-User}}^{\text{HD}}$  (resp.  $\tilde{r}_{\text{BS-BS}}^{\text{FD}}/r_{\text{BS-BS}}^{\text{HD}}$ ).

# 4.4 FD Link Objective

Our objective is to maximize the FD rate gains in the two FD use cases. In particular, based on the observation above, our goal is to obtain the optimal FD Tx and Rx beamformers,  $\mathbf{w}$  and  $\mathbf{v}$ , that maximize TxBF and RxBF gains,  $g_{\rm t}$  and  $g_{\rm r}$ , while achieving sufficient amount of RF SIC, i.e.,

 $\gamma_{bb}(f_k) \leq 1 \Leftrightarrow |\mathbf{v}^{\mathsf{T}}\mathbf{H}(f_k)\mathbf{w}|^2 \cdot \frac{P_{\mathsf{t}}}{N} \leq SIC_{\mathsf{dig}} \cdot (NP_{\mathsf{nf}}) := N\beta, \quad (15)$  where  $\beta := SIC_{\mathsf{dig}}P_{\mathsf{nf}}$  is a constant independent of N and  $P_{\mathsf{t}}$ . Moreover, in order to (i) preserve the phase of the signals (i.e., the Tx and Rx array factors,  $a_{\mathsf{t}}$  and  $a_{\mathsf{r}}$ , should only contain real parts), and (ii) to balance the TxBF and RxBF gains in the far-field (i.e.,  $g_{\mathsf{t}} = g_{\mathsf{r}}$  so that the Tx and Rx signals do not experience different power level changes), the following constraints are set based on (3)–(4):

$$\begin{cases} (i) \ a_t, a_r \in \mathbb{R} \Leftrightarrow Im[a_t] = Im[a_r] = 0 \text{ (no phase offset),} \\ (ii) \ g_t = g_r \Leftrightarrow a_t = a_r \text{ (balanced TxBF and RxBF gains).} \end{cases}$$
(16)

Next, we first present the benefits introduced by FD phased arrays in terms of FD rate gains (Section 5). Then, we present the corresponding problem formulation (Section 6).

#### 5 MOTIVATING EXAMPLES

In this section, we illustrate the FD rate gains obtained by FD phased arrays with joint TxBF and RxBF, where the FD rate gains are computed as described in Section 4.3. We provide several examples illustrating that higher values of the optimal FD TxBF and RxBF gain lead to increased FD rate gains. According to Sections 4.2 and 4.4, we let  $g_t^{\star} = g_t^{\star} = g^{\star}$  with the corrsponding  $a_t^{\star} = a_t^{\star} = a^{\star} \in \mathbb{R}$ 

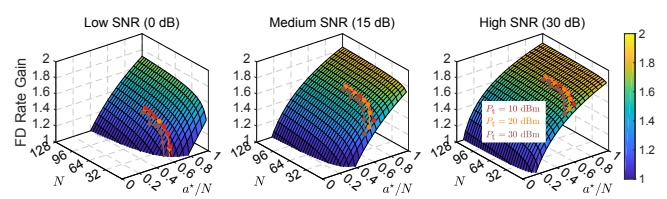


Figure 4: FD rate gain in the BS-User case with varying number of antennas, N, and the normalized optimal FD Tx and Rx array factors,  $a^*/N$ , for different link SNR values  $y \in \{0, 15, 30\}$  dB. The relationships between  $a^*/N$  and N, based on the Argos traces [1], are also overlayed on the surface with  $P_t \in \{10, 20, 30\}$  dBm.

satisfying  $g^* = (a^*)^2/N$  (see (16)). We will describe how to obtain  $a^*$  (and thus  $q^*$ ) in Section 6.

**BS-User Case**: We first consider equal UL and DL SNR values of  $\gamma_{bu} = \gamma_{ub} = \gamma$  in low, medium, and high SNR regimes with  $\gamma \in \{0, 15, 30\}$  dB. These values correspond to typical Rx signal levels in an LTE network, where the user is at the edge, middle, and center of the small cell. Fig. 4 presents the FD rate gain with varying number of antennas,  $N \in \{4, 8, \ldots, 128\}$ , and the *normalized* optimal FD Tx and Rx array factor  $a^*/N \in [0, 1]$ .

Fig. 4 shows, for example, that a 16-element FD phased array can achieve FD rate gains of  $1.13/1.55/1.71\times$  in low/medium/high SNR regimes, with 3 dB TxBF and RxBF gain loss (i.e.,  $g^* = 0.5N$  and  $a^* = \frac{\sqrt{2}}{2}N$ ). These rate gains increase to  $1.35/1.63/1.75\times$  when N = 64. Moreover, with 6 dB TxBF and RxBF gain losses, a 64-element FD phased array can achieve FD rate gains of  $1.05/1.46/1.62\times$  in low/medium/high SNR regimes. As we will show in Section 7, a TxBF and RxBF gain loss of 6 dB is sufficient to achieve  $\gamma_{bb}(f_k) \le 1, \forall k$ , in most considered scenarios. It is also interesting to note that under sufficient link SNR values, an FD phased array with more antennas provides marginal improvements on the FD rate gain. For example, in the medium SNR regime, N = 64/128 elements can achieve FD rate gains of  $1.63/1.66\times$ , respectively (namely, doubling the number of antennas provides an improvement of only 3%).

To provide a practical example of the FD rate gain, we overlay in Fig. 4 curves that represent relationships between  $a^*/N$  and N using  $H(f_k)$  from the Argos dataset [1] with different Tx power levels (the details will be described in Section 7.4 and shown in Fig. 11). For example, the Argos array with  $P_t = 20$  dBm can achieve  $a^*/N = 0.66/0.69/0.70$  for N = 18/36/72. In addition, the Argos array with  $P_t = 20$  dBm and N = 36 experiences only 3.1 dB TxBF and RxBF gain losses each, and can achieve maximum FD rate gains of  $1.27/1.60/1.72\times$  in low/medium/high SNR regimes. Importantly, the curves show that in a given FD phased array with given values of N and  $P_t$ , there exists an upper limit of  $a^*$  on  $a_t$  and  $a_r$  that any FD Tx and Rx beamformers cannot exceed. Since the FD rate gain increases as a function of  $g^* = (a^*)^2/N$  (see (13)–(14)), designing FD Tx and Rx beamformers that reach the upper limit of  $a^*$  will result in the maximum achievable FD rate gain.

We also evaluate the FD rate gain with asymmetric UL and DL SNR values, a scenario which is more common in realistic network settings. Fig. 5 presents the FD rate gain with varying UL and DL SNR values,  $\gamma_{bu}$  and  $\gamma_{ub}$ , with  $N \in \{16,32\}$  and with 3 dB TxBF and RxBF gain loss, respectively. The results show that FD rate gains of  $1.14 \times -1.71 \times /1.26 \times -1.73 \times$  can be achieved with N = 16/32 under all considered UL and DL SNR values. Note that the FD rate gain also increases as a function of the number of antennas, N.

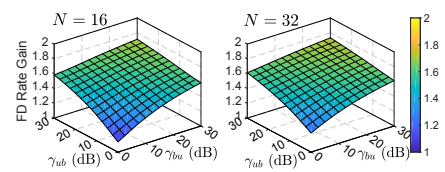


Figure 5: FD rate gain in the BS-User case with varying UL and DL SNR values,  $\gamma_{bu}$  and  $\gamma_{ub}$ , respectively, with  $N \in \{16, 32\}$  and  $3 \, \mathrm{dB}$  TxBF and RxBF gain loss (i.e.,  $g^* = N/2$ ).

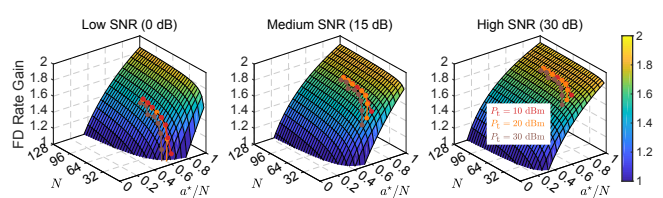


Figure 6: FD rate gain in the BS-BS case with varying number of antennas, N, and the normalized optimal FD Tx and Rx array factors,  $a^*/N$  for different link SNR values  $\gamma \in \{0, 15, 30\}$  dB. The relationships between  $a^*/N$  and N, based on the Argos traces [1], are also overlayed on the surface with  $P_t \in \{10, 20, 30\}$  dBm.

**BS-BS Case**: Fig. 6 plots the FD rate gain in the BS-BS case with the same setting as used in the BS-User case. The results show that a 16-element FD phased array can achieve FD rate gains of  $1.25/1.53/1.66\times$  in low/medium/high SNR regimes, with only 3 dB TxBF and RxBF gain loss. These gains increase to  $1.49/1.64/1.72\times$  with N=64. The curves representing the relationships between  $a^*/N$  and N using the Argos traces are overlayed in Fig. 6, and similar observations as in the BS-User case are also relevant in the BS-BS case. In both use cases, the FD rate gain does not approach  $2\times$ , due to the XINR at the BS and user,  $\gamma_{bb} = \gamma_{uu} = 1$ .

Findings. As indicated above, although an FD phased array experiences TxBF and RxBF gain losses in the desired beam-pointing directions to achieve  $\gamma_{bb}(f_k) \leq 1$ , the network can still achieve significant FD rate gains in various settings. Therefore, it is important to obtain the optimal Tx and Rx array factors,  $a_t^{\star}$  and  $a_r^{\star}$ , in an FD phased array in order to achieve high FD rate gain in the considered use cases. The results also reveal an interesting phenomenon: with increased number of antennas, N, minimal TxBF and RxBF gain losses (e.g., 3 dB) do not affect the achieved FD rate gains. In addition, higher TxBF and RxBF gain losses are needed in order to achieve sufficient SIC under different Tx power level,  $P_t$ , and bandwidth, B, requirements, as we will show in Section 7. This tradeoff opens up a possibility of designing FD phased arrays with different geometries and/or values of N under varying system requirements (e.g., Tx power levels, link SNRs, bandwidth).

#### 6 FORMULATION AND OPTIMIZATION

In this section, we formulate an optimization problem based on the FD link objective described in Section 4.4. Due to the non-convexity and computational complexity of the problem, we then present an alternative formulation whose solution can be efficiently obtained using an iterative algorithm with provable performance guarantees.

#### 6.1 Problem Formulation

Based on the FD link objective defined in Section 4.4, the following problem jointly determines the FD Tx and Rx beamformers.

$$(Opt-TxRx) a^* := \max_{\mathbf{w}, \mathbf{v}} a \tag{17}$$

s.t. : 
$$Re[\mathbf{s}_{t}^{\mathsf{T}}\mathbf{w}] = a$$
,  $Im[\mathbf{s}_{t}^{\mathsf{T}}\mathbf{w}] = 0$ , (18)

$$Re[\mathbf{s}_{\mathbf{r}}^{\mathsf{T}}\mathbf{v}] = a, \ Im[\mathbf{s}_{\mathbf{r}}^{\mathsf{T}}\mathbf{v}] = 0, \tag{19}$$

$$P_{SI}^{bf}(f_k) = |\mathbf{v}^{\top} \mathbf{H}(f_k) \mathbf{w}|^2 \cdot \frac{P_t}{N} \le N\beta, \ \forall k, \quad (20)$$

$$|w_n|^2 \le 1, \ |v_n|^2 \le 1, \ \forall n.$$
 (21)

Specifically, the objective (17) is to maximize the Tx and Rx array factors, subject to the following constraints (see Section 4.4):

- (i) The Tx and Rx array factors in the desired beam-pointing directions,  $(\phi_t, \theta_t)$  and  $(\phi_r, \theta_r)$ , have equal *real* responses, (18)–(19);
- (ii) The residual SI power at any frequency is suppressed to below the array noise floor, i.e.,  $\gamma_{bb}(f_k) \leq 1$ ,  $\forall k$ , (20);
- (iii) The amplitude of the beamforming weight on each Tx/Rx element is at most one (see Section 3), (21).

Essentially, the Tx and Rx beamformers that are obtained as a solution are different from the conventional HD beamfomers such that the total SI power is canceled to below the array noise floor with minimal TxBF and RxBF gain loss. In order words, TxBF and RxBF are repurposed for achieving wideband RF SIC. Throughout the paper, we practically set  $P_{\rm nf} = -90$  dBm and  $SIC_{\rm dig} = 40$  dB. Therefore, according to (15),  $\beta = P_{\rm nf} \cdot SIC_{\rm dig} = -90$  dBm + 40 dB = -50 dBm =  $10^{-5}$  mW.

Note that (18)–(19) are linear constraints, and (21) is a convex (non-linear) constraint. Moreover, (Opt-TxRx) always has a feasible solution where  ${\bf w}$  and  ${\bf v}$  have very small amplitudes. However, in general, (Opt-TxRx) is a *non-convex* optimization problem whose solution poses several challenges. The non-convexity stems from the coupling between  ${\bf w}$  and  ${\bf v}$  through  ${\bf H}(f_k)$  in (20) where  ${\bf H}(f_k)$  is not a Hermitian matrix, and not even a symmetric matrix in realistic environments (see Section 4.1). Moreover, the problem becomes computationally expensive to solve using existing solvers (which may only return a local optimum) with increased number of antennas, N, especially for massive-antenna systems and large-scale phased arrays. For benchmarking purposes, in Section 7, we use the nonlinear programming solver from MATLAB to solve (Opt-TxRx) and denote the returned (possibly only locally) optimal FD Tx and Rx array factors by  $a_t^*$  and  $a_r^*$ , respectively.

## 6.2 Observation and Intuition

Due to the intractability of (Opt-TxRx), we now describe alternative optimization problems which are based on the observation below. Note that the SI power in (20) can be written as,

$$P_{SI}^{bf}(f_k) = |\mathbf{v}^{\top}\mathbf{H}(f_k)\mathbf{w}|^2 \cdot \frac{P_t}{N} = (\mathbf{v}^{\top}\mathbf{H}(f_k)\mathbf{w})^{\dagger} \cdot (\mathbf{v}^{\top}\mathbf{H}(f)\mathbf{w}) \cdot \frac{P_t}{N}$$

$$= \mathbf{w}^{\dagger} \left( \underbrace{\mathbf{H}^{\dagger}(f_k)\mathbf{v}^*\mathbf{v}^{\top}\mathbf{H}(f_k)}_{:=\mathbf{H}_{\mathbf{v}}(f_k)} \right) \mathbf{w} \cdot \frac{P_t}{N} = \mathbf{w}^{\top}\mathbf{H}_{\mathbf{v}}(f_k)\mathbf{w} \cdot \frac{P_t}{N}, \ \forall k.$$

It can be seen that with a fixed Rx beamformer, v,

- $\mathbf{H}_{\mathbf{v}}(f_k)$  is a *Hermitian* matrix, i.e.,  $\mathbf{H}_{\mathbf{v}}(f_k) = \mathbf{H}_{\mathbf{v}}^{\mathsf{T}}(f_k), \forall k$ ;
- H<sub>v</sub>(f<sub>k</sub>) is positive semidefinite since, for any non-zero Tx beamformer, w, the SI power cannot be negative, i.e.,

$$\mathbf{w}^{\dagger} \mathbf{H}_{\mathbf{V}}(f_k) \mathbf{w} \cdot \frac{P_t}{N} \ge 0, \ \forall k, \ \forall \mathbf{w} \in \mathbb{C}^N \ \text{and} \ \mathbf{w} \ne \mathbf{0}.$$

 $<sup>^3</sup>$  Recent work has demonstrated  $SIC_{\rm dig}=43/50~{\rm dB}$  [6, 9] which leads to more relaxed requirements on the amount of RF SIC.

<sup>&</sup>lt;sup>4</sup>Due to the non-convexity of (Opt-TxRx), we use the same  $a_{\rm t}^{\star}$  and  $a_{\rm r}^{\star}$  as in Section 4.2 to denote the numerically obtained solution to (Opt-TxRx) using existing solvers.

Therefore, the optimal Tx beamformer that maximizes the Tx array factor,  $a_t$ , given a fixed v, can be obtained by solving (P1):

(P1) 
$$\max_{\mathbf{w}} a_t$$
, s.t. :  $\text{Re}[\mathbf{s}_t^{\top} \mathbf{w}] = a_t$ ,  $\text{Im}[\mathbf{s}_t^{\top} \mathbf{w}] = 0$ ,

$$\mathbf{w}^{\dagger}\mathbf{H}_{\mathbf{v}}(f_k)\mathbf{w}\cdot\frac{P_{\mathbf{t}}}{N}\leq N\beta, \forall k, \ |w_n|^2\leq 1, \ \forall n.$$

Unlike (Opt-TxRx), this is a *quadratically constrained convex program*, since  $H_{\mathbf{v}}(f_k)$  is a Hermitian matrix. Symmetrically, the optimal Rx beamformer that maximizes the Rx array factor given a fixed Tx beamformer  $\mathbf{w}$ , can be obtained by solving (P2):

(P2) 
$$\max_{\mathbf{v}} a_{\mathbf{r}}$$
, s.t. :  $\text{Re}[\mathbf{s}_{\mathbf{r}}^{\top}\mathbf{v}] = a_{\mathbf{r}}$ ,  $\text{Im}[\mathbf{s}_{\mathbf{r}}^{\top}\mathbf{v}] = 0$ ,

$$\mathbf{v}^{\dagger}\mathbf{H}_{\mathbf{w}}(f_k)\mathbf{v}\cdot\frac{P_{\mathbf{t}}}{N}\leq N\beta,\ \forall k,\ |v_n|^2\leq 1,\ \forall n.$$

(P1) and (P2) are convex programs that can be solved efficiently via existing solvers (e.g., CVX). Intuitively, an algorithm that updates w and v by iteratively solving (P1) and (P2) can be applied, i.e., solving for v given fixed w, and then solving for an updated w with the newly obtained v. However, the obtained TxBF and RxBF gains can be largely imbalanced since w and v are updated *independently*.

#### 6.3 The Iterative Algorithm

We now present an iterative algorithm (described in Algorithm 1) that simultaneously maximizes and balances the Tx and Rx array factors.  $^5$  Let  $\kappa \in \mathbb{Z}$  be the index of iteration. Let  $\mathbf{w}^{(0)}$  and  $\mathbf{v}^{(0)}$  be the initial Tx and Rx beamformers with corresponding Tx and Rx array factors of  $a_{\mathrm{t}}^{(0)}$  and  $a_{\mathrm{r}}^{(0)}$ , respectively. Let  $\mathbf{w}^{(\kappa)}$  and  $a_{\mathrm{t}}^{(\kappa)}$  (resp.  $\mathbf{v}^{(\kappa)}$  and  $a_{\mathrm{r}}^{(\kappa)}$ ) be the optimal Tx (resp. Rx) beamformer and Tx (resp. Rx) array factor obtained by the iterative algorithm in the  $\kappa^{\mathrm{th}}$  iteration. For  $\kappa \in \mathbb{Z}$ , we define the following two objective functions.

$$F_{t}^{(\kappa+1)}(a_{t}) = a_{t} - \alpha_{\kappa+1} \cdot (a_{t} - a_{r}^{(\kappa)})^{2},$$

$$F_{r}^{(\kappa+1)}(a_{r}) = a_{r} - \alpha_{\kappa+1} \cdot (a_{r} - a_{s}^{(\kappa+1)})^{2},$$
(22)

where  $\alpha_{\kappa+1}$  is the *step size*. Essentially, in the  $(\kappa+1)^{\text{th}}$  iteration, a penalty term is introduced, which is the square of the difference between the Tx and Rx array factors with a weighting factor of  $\alpha_{\kappa+1}$ . Therefore, Tx and Rx array factors with a larger difference will prevent their individual value from increasing rapidly.

To allow analytical tractability and easy implementation of the developed iterative algorithm, it is important to properly select: (i) the initial Tx and Rx beamformers,  $\mathbf{w}^{(0)}$  and  $\mathbf{v}^{(0)}$ , and (ii) the sequence of step size,  $\{\alpha_K\}_{K\in\mathbb{Z}}$ . In particular, we set:

sequence of step size, 
$$\{\alpha_{\kappa}\}_{\kappa \in \mathbb{Z}}$$
. In particular, we set:  

$$\mathbf{w}^{(0)} = \frac{\beta^{1/4} \cdot \mathbf{w}_{\text{conv}}}{2P_t^{1/4} N^{1/2}}, \ \mathbf{v}^{(0)} = \frac{\beta^{1/4} \cdot \mathbf{v}_{\text{conv}}}{2P_t^{1/4} N^{1/2}}, \ \text{and} \ \alpha_{\kappa} = \frac{1}{\kappa^2}, \ \forall \kappa.$$
 (23)

We also note that the above choices of  $\mathbf{w}^{(0)}$ ,  $\mathbf{v}^{(0)}$ , and  $\{\alpha_{\kappa}\}$  are *not unique*. For example, any step size sequence  $\{\alpha_{\kappa}\}$  satisfying  $1 = \alpha_1 \ge \alpha_2 \ge \cdots > 0$  also suffices. In Section 7, we will evaluate the effect of  $\{\alpha_{\kappa}\}$  on the solution obtained by the iterative algorithm.

#### 6.4 Performance Analysis

In this section, we analyze the performance of the iterative algorithm. We first present the following lemma about the structural properties of the objective functions of (Opt-Tx) and (Opt-Rx) in (22). Then, we state the main results in Proposition 6.1. For proofs see supplementary materials.

Lemma 6.1. Under the iterative algorithm, 
$$\forall \kappa \in \mathbb{Z}$$
, 
$$\frac{F_t^{(\kappa+1)}(a_t^{(\kappa+1)})}{F_t^{(\kappa+1)}(a_t^{(\kappa)})} \geq F_t^{(\kappa+1)}(a_t^{(\kappa)}), \ F_r^{(\kappa+1)}(a_r^{(\kappa+1)}) \geq F_r^{(\kappa+1)}(a_r^{(\kappa)}).$$
5 The idea of the developed iterative algorithm is similar to that presented in [4].

#### **Algorithm 1** The Iterative Algorithm

**Input and Initialization**: N,  $P_t$ ,  $H(f_k)$ ,  $\forall k$ ,  $s_t = s(\phi_t, \theta_t)$ , and  $s_r = s(\phi_r, \theta_r)$ . Initial values of Tx and Rx beamformers  $\mathbf{w}^{(0)}$  and  $\mathbf{v}^{(0)}$ , respectively. The step size sequence,  $\{\alpha_\kappa\}_{\kappa\in\mathbb{Z}}$ .

For  $\kappa = 0, 1, \cdots$  do

1: Obtain  $\mathbf{w}^{(\kappa+1)}$  with given  $\mathbf{v}^{(\kappa)}$  and  $a_{\mathrm{r}}^{(\kappa)}$  by solving

$$\begin{split} \text{(Opt-Tx)} \ a_{\mathrm{t}}^{(\kappa+1)} \coloneqq & \arg\max_{\mathbf{w}} \ F_{\mathrm{t}}^{(\kappa+1)}(a_{\mathrm{t}}) = a_{\mathrm{t}} - \alpha_{\kappa+1} \cdot (a_{\mathrm{t}} - a_{\mathrm{r}}^{(\kappa)})^2 \\ \text{s.t.} \ : & \mathrm{Re}[\mathbf{s}_{\mathrm{t}}^{\top}\mathbf{w}] = a_{\mathrm{t}}, \ & \mathrm{Im}[\mathbf{s}_{\mathrm{t}}^{\top}\mathbf{w}] = \mathbf{0}, \\ & \mathbf{w}^{\dagger}\mathbf{H}_{-(\kappa)}(f_{k})\mathbf{w} \cdot \frac{P_{\mathrm{t}}}{N} \leq N\beta, \ \forall k, \ & |w_{n}|^{2} \leq 1, \ \forall n. \end{split}$$

2: Obtain 
$$\mathbf{v}^{(\kappa+1)}$$
 with given  $\mathbf{w}^{(\kappa+1)}$  and  $a_{\mathbf{t}}^{(\kappa+1)}$  by solving

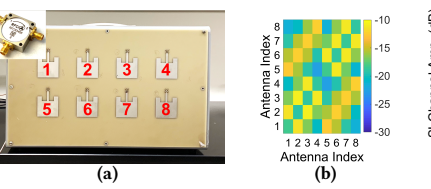
(Opt-Rx) 
$$a_{\rm r}^{(\kappa+1)} := \arg\max_{\bf r} \ F_{\rm r}^{(\kappa+1)}(a_{\rm r}) = a_{\rm r} - \alpha_{\kappa+1} \cdot (a_{\rm r} - a_{\rm t}^{(\kappa+1)})^2$$

s.t. : 
$$Re[\mathbf{s}_r^{\mathsf{T}}\mathbf{v}] = a_r$$
,  $Im[\mathbf{s}_r^{\mathsf{T}}\mathbf{v}] = 0$ ,

$$\mathbf{v}^{\dagger}\mathbf{H}_{\mathbf{w}(\kappa+1)}(f_k)\mathbf{v}\cdot\frac{P_{\mathbf{t}}}{N}\leq N\beta, \ \forall k, \ |\upsilon_n|\leq 1, \ \forall n.$$

3: Keep iterating until the Tx and Rx array factor improvements are within  $\delta N$ , i.e.,

$$\max \left\{ a_{\mathbf{t}}^{(\kappa+1)} - a_{\mathbf{t}}^{(\kappa)}, \, a_{\mathbf{r}}^{(\kappa+1)} - a_{\mathbf{r}}^{(\kappa)} \right\} \le \delta \cdot N. \tag{24}$$



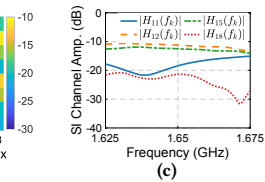


Figure 7: (a) A customized 1.65 GHz 8-element rectangular array and the RFCR3206 circulator, (b) the measured  $|H_{mn}(f_k)|$  at 1.65 GHz, and (c) the amplitudes of some example SI channels,  $|H_{mn}(f_k)|$ .

Recall that 
$$g_t^{(\kappa)} = (a_t^{(\kappa+1)})^2/N$$
 and  $g_r^{(\kappa)} = (a_r^{(\kappa+1)})^2/N$ .

PROPOSITION 6.1. With initial Tx and Rx beamformers,  $\mathbf{w}^{(0)}$  and  $\mathbf{v}^{(0)}$ , and step size,  $\alpha_K$ , given in (23), under the iterative algorithm,

$$a_t^{(\kappa+1)} \ge a_t^{(\kappa)} \text{ and } a_r^{(\kappa+1)} \ge a_r^{(\kappa)}, \ \forall \kappa \in \mathbb{Z}.$$
 (25)

Furthermore, the corresponding TxBF and RxBF gains satisfy, 
$$\forall \kappa \in \mathbb{Z}$$
,  $g_t^{(\kappa+1)} \geq g_t^{(\kappa)}, \ g_t^{(\kappa+1)} \geq g_r^{(\kappa)}, \ g_t^{(\kappa+1)} + g_r^{(\kappa+1)} \geq g_t^{(\kappa)} + g_r^{(\kappa)}$ . (26)

**Remark**: Proposition 6.1 states that after each iteration, the obtained Tx and Rx array factors,  $a_{\rm t}^{(\kappa)}$  and  $a_{\rm r}^{(\kappa)}$ , are guaranteed to be no smaller than their values in the previous iteration. From condition (24) and fact that  $a_{\rm t}^{\rm max}=a_{\rm r}^{\rm max}=N$ , it can be seen that Algorithm 1 will terminate within at most  $\left\lceil \frac{N}{\delta \cdot N} \right\rceil = \left\lceil \frac{1}{\delta} \right\rceil$  iterations.

# 7 MEASUREMENT-BASED EVALUATION

In this section, we first describe the measurements, datasets, and setup. Then, we numerically evaluate the performance of an FD phased array with TxBF and RxBF and discuss design tradeoffs.

#### 7.1 Measurements and Datasets

Since currently large-scale Tx and Rx phased array nodes are not widely available, our evaluations are based on  $\mathbf{H}(f_k)$  from measurements and traces. In particular, we consider two antenna arrays as described below with different array geometries, number of antennas, N, and bandwidth, B.

A Customized Rectangular Array with Circulators. We custom designed a 1.65 GHz 8-element rectangular antenna array using a slot loop antenna structure as shown in Fig. 7(a). The spacing between adjacent antennas is half-wavelength. An RF-CI RFCR3406 circulator is also included (see Fig. 3). We measure the frequency



Figure 8: (a) The 2.4 GHz 72-element Argos hexagonal array for which the SI channel measurements were reported in [1, 16], (b) the Taoglas 2.4 GHz circular antenna, and (c) the measured amplitude of the antenna response that is used for  $|H_{nn}(f_k)|$ ,  $\forall n$ .

responses of the antenna array and the circulator, from which the SI channel matrix,  $\mathbf{H}(f_k) \in \mathbb{C}^{8\times 8}$ , is constructed. In particular,  $\mathbf{H}(f_k)$ , is measured using a vector network analyzer at frequencies between 1.625–1.675 GHz (B=50 MHz). Figs. 7(b) and 7(c) respectively plot the measured  $|H_{mn}(f_k)|$  at  $f_k=1.65$  GHz, and example SI channels,  $|H_{mn}(f_k)|$ , with high frequency-selectivity.

The Argos Hexagonal Array [1, 23]. We also leverage the publicly available Argos dataset from [1, 23]. The Argos platform consists of 72 circular patch antennas at 2.4 GHz placed in a hexagonal grid consisting of 8 rows and 9 columns, with 0.6-wavelength spacing between adjacent elements (see Fig. 8(a)). The SI channel matrix,  $\mathbf{H}(f_k) \in \mathbb{C}^{72\times 72}$ , is measured using a WARPv3 platform with B=20 MHz bandwidth and K=64 subcarriers (52 non-zero subcarriers). With such a large number of antennas, uniform linear arrays (ULAs) and hexagonal planar arrays with different values of N can be constructed by taking a subset of the measurements.

However, the Argos platform employs seperate Tx and Rx antennas and does not contain circulators. Therefore,  $\mathbf{H}(f_k)$  is missing the diagonal elements,  $H_{nn}(f_k)$ ,  $\forall n$ . To complete  $\mathbf{H}(f_k)$ , we measure the frequency response of a Taoglas 2.4 GHz circular antenna (see Fig. 8(b)). Using the completed  $\mathbf{H}(f_k)$ , we generate hexagonal arrays with  $N \in \{9,\ldots,72\}$  by considering the top  $\{1,\ldots,8\}$  rows of the Argos array. Note that case of N=9 corresponds to a ULA. **Steering Vectors of the Rectangular and Argos Arrays**. The steering vector of the rectangular array is computed as described in Section 3. The steering vector of the Argos hexagonal array is given by  $(n=(n_X-1)N_y+n_y)$ 

$$s_n(\phi, \theta) = \begin{cases} e^{j\frac{6\pi}{5}[(n_x - 1)\cos\theta\cos\phi + \frac{\sqrt{3}}{2}(n_y - 1)\cos\theta\sin\phi]}, & n_y \text{ odd,} \\ e^{j\frac{6\pi}{5}[(n_x - \frac{1}{2})\cos\theta\cos\phi + \frac{\sqrt{3}}{2}(n_y - 1)\cos\theta\sin\phi]}, & n_y \text{ even.} \end{cases}$$

Our evaluations using the Argo dataset is with B=20 MHz as provided [1, 23]. For higher bandwidth up to B=50 MHz, we use the rectangular array measurements. For compactness of presentation, unless mentioned otherwise, we use  $N\in\{8,9,18,\ldots,72\}$  to correspond to different array geometries. Note that in both antenna arrays, the measured  $\mathbf{H}(f_k)$  is neither Hermitian nor symmetric although Fig. 7(b) presents some level of symmetry.

#### 7.2 Setup

**TxBF and RxBF in HD and FD modes**. We consider TxBF and RxBF in the *front side* of the antenna array with  $\phi \in [-180^{\circ}, 180^{\circ}]$  and  $\theta \in [0^{\circ}, 90^{\circ}]$ . Specifically, the array *broadside* corresponds to the direction of  $\theta = 90^{\circ}, \forall \phi$  (see Fig. 2(a)). We consider  $P_t \in \{10, 20, 30\}$  dBm<sup>6</sup>, and  $P_{\rm nf} = -90$  dBm and  $SIC_{\rm dig} = 40$  dB (see Section 4.4). The FD rate gains are computed as described in Section 4.3.

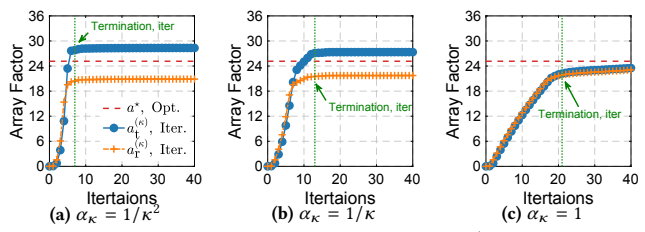


Figure 9: The optimal Tx and Rx array factors,  $a^*$ , and the Tx and Rx array factors obtained the by iterative algorithm,  $a_{\mathbf{t}}^{(\kappa)}$  and  $a_{\mathbf{r}}^{(\kappa)}$ , with N=36,  $P_{\mathbf{t}}=20$  dBm, and different step sizes,  $\{\alpha_{\kappa}\}$ .

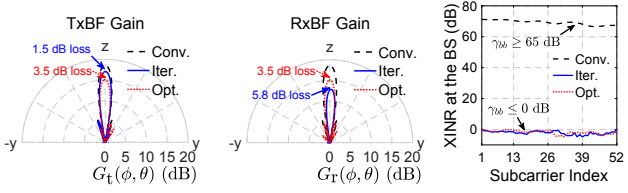


Figure 10: TxBF and RxBF gains, and the resulting XINR under different TxBF and RxBF, with N=72,  $P_{\rm t}=30~{\rm dBm}$ , and the Tx and Rx beam-pointing directions in the array broadside (i.e., z-axis).

The following TxBF and RxBF schemes are considered:

- (1) Conventional HD TxBF and RxBF (Conv.), which is based on (5) and achieves  $a_r^{\text{max}} = a_r^{\text{max}} = N$  and  $g_r^{\text{max}} = g_r^{\text{max}} = N$ ;
- (2) Optimal FD TxBF and RxBF (Opt.), which is based on solving (Opt-TxRx). Recall that the obtained (equal) optimal Tx and Rx array factor is denoted by a\*, and corresponds to the (equal) optimal TxBF and RxBF gain of g\*;
- (3) Iterative FD TxBF and RxBF (**Iter.**), which is based on the iterative algorithm with  $\delta = 0.01$  set in the termination step. Denote by  $\widetilde{a_t}$  (resp.  $\widetilde{a_r}$ ) the returned Tx (resp. Rx) array factor and by  $\widetilde{g_t}$  (resp.  $\widetilde{g_r}$ ) the corresponding TxBF (resp. RxBF) gain, respectively. The evaluations are performed using a laptop with a quad-core Intel i7 CPU and 16GB RAM. For the optimal Tx FD TxBF and RxBF, we apply the nonlinear solver in MATLAB. For the iterative FD

TxBF and RxBF, we apply the MATLAB CVX solver in each iteration

for solving the convex (Opt-Tx) and (Opt-Rx) (see Section 6).

**Selecting the Step Size**,  $\{\alpha_{\kappa}\}$ . To study the impact of  $\{\alpha_{\kappa}\}$ , we remove the termination condition in the iterative algorithm and record the obtained  $a_{\rm t}^{(\kappa)}$  and  $a_{\rm r}^{(\kappa)}$ . We consider N=36 and  $P_{\rm t}=20$  dBm, and three different step sizes satisfying the conditions specified in Section 6.3: (i)  $\alpha_{\kappa}=1/\kappa^2$ , (2)  $\alpha_{\kappa}=1/\kappa$ , and (iii)  $\alpha_{\kappa}=1$  (constant). Fig. 9 plots the obtained  $a_{\rm t}^{(\kappa)}$  and  $a_{\rm r}^{(\kappa)}$  over iterations,  $\kappa$ , and the optimal Tx and Rx array factor,  $a^{\star}$ . The results show that under all considered three choices of  $\{\alpha_{\kappa}\}$ ,  $a_{\rm t}^{(\kappa)}$  and  $a_{\rm r}^{(\kappa)}$  converge within 25 iterations. However,  $a_{\rm t}^{(\kappa)}$  and  $a_{\rm r}^{(\kappa)}$  become more imbalanced with more aggressive step sizes (e.g.,  $\alpha_{\kappa}=1/\kappa^2$ ). The results for other values of N and  $P_{\rm t}$  also reveal similar trends. Therefore, we empirically set  $\alpha_{\kappa}=1/\kappa^2$ ,  $\forall \kappa$ , which achieves fast termination (e.g., less than 10 iterations for all values of N,  $P_{\rm t}$ , and B considered) and for which the obtained  $\widetilde{g_{\rm t}}$  are relatively well balanced.

# 7.3 XINR and Gain Loss under TxBF and RxBF

We now evaluate the XINR at the BS,  $\gamma_{bb}(f_k)$ , under different TxBF and RxBF. We consider N=72 and  $P_t=30$  dBm with the desired Tx and Rx beam-pointing directions in the array broadside. Fig. 10 plots

<sup>&</sup>lt;sup>6</sup>These values correspond to the typical Tx power levels of a BS in a small/micro cell.

 $<sup>^7</sup>$ The returned solution to (Opt-TxRx) may be locally optimal due to its non-convexity.

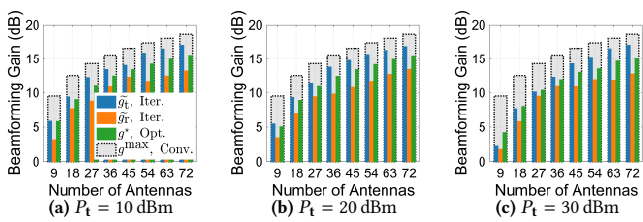


Figure 11: TxBF and RxBF gains under different TxBF and RxBF with varying number of antennas, N, and  $P_t \in \{10, 20, 30\}$  dBm.

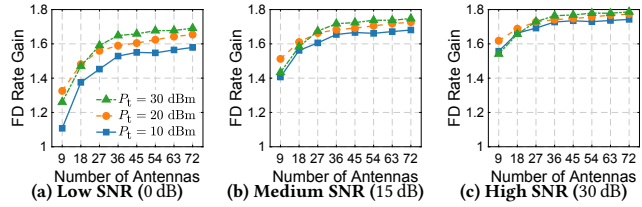


Figure 12: FD rate gain in the BS-BS case when both BSs face each other in the broadside, with varying number of antennas, N, and  $P_t \in \{10, 20, 30\} \, \text{dBm}$ , in the low/medium/high SNR regimes.

Table 1: Average ratio between the FD rate gains achieved under the iterative (with  $\widetilde{g_t}$  and  $\widetilde{g_r}$ ) and optimal (with  $g^\star$ ) TxBF and RxBF

Avg. ratio b/w FD rate gains under $(\widetilde{g}_t, \widetilde{g}_r)$ and $g^*$	N = 9	<i>N</i> = 18	N = 27	N = 36	$N \ge 45$
Low SNR (0 dB)	0.89	0.95	0.97	0.98	≥ 0.98
Medium SNR (15 dB)	0.93	0.97	0.98	0.99	≥ 0.99
High SNR (30 dB)	0.95	0.98	0.98	0.99	≥ 0.99

the TxBF and RxBF gains (see (2)) and the XINR,  $\gamma_{bb}(f_k)$ , under different TxBF and RxBF. It can be seen that the HD TxBF and RxBF results in extremely high XINR of  $\gamma_{bb}(f_k) \geq 65$  dB,  $\forall k$ , thereby FD operation at the BS cannot be supported. Both the optimal and iterative TxBF and RxBF are able to cancel the SI power to below the array noise floor, i.e.,  $\gamma_{bb}(f_k) \leq 1$  (0 dB). The corresponding TxBF and RxBF gain losses associated with the optimal/iterative TxBF and RxBF are only 3.5 dB/1.5 dB and 3.5 dB/5.8 dB, respectively.

## 7.4 FD TxBF and RxBF Gains and Rate Gain

**FD TxBF and RxBF Gains**. We first evaluate the FD TxBF and RxBF gains. We consider Tx and Rx beam-point directions in the array broadside with  $N \in \{9, 18, \ldots, 72\}$  and  $P_t \in \{10, 20, 30\}$  dBm. Fig. 11 plots the optimal FD TxBF and RxBF gain,  $g^*$ , and the iterative FD TxBF and RxBF gains,  $\widetilde{g_t}$  and  $\widetilde{g_r}$ , respectively. The conventional HD TxBF and RxBF gains of N are also plotted.

The results show that for a given number of antennas, N, the TxBF and RxBF gain losses are more significant with increased Tx power level,  $P_{\rm t}$ . For a given value of  $P_{\rm t}$ , the TxBF and RxBF gain losses decrease with a larger number of antennas, N. For example, an FD phased array with  $P_{\rm t}=20\,{\rm dBm}$  and N=72 experiences 1.7 dB and 5.1 dB TxBF and RxBF gain losses, respectively. These values are only marginally changed to 1.8 dB and 5.7 dB with N=36. The iterative algorithm achieves relative balanced FD TxBF and RxBF gains across varying N. Specifically,  $\widetilde{g}_{\rm t}$  and  $\widetilde{g}_{\rm r}$  are always within  $\pm 2.8\,{\rm dB}$  of the optimal FD TxBF and RxBF gain,  $g^{\star}$ . Moreover,  $\gamma_{bb}(f_k) \leq 1$ ,  $\forall k$ , can be achieved with at most 8.0/8.2/11.6 dB sum TxBF and RxBF gain loss for  $P_{\rm t}=10/20/30\,{\rm dBm}$  when  $N\geq 18$ .

**BS-BS Case**. We consider the FD rate gain when both BSs face each other in the array braodside. Fig. 12 plots the FD rate gains

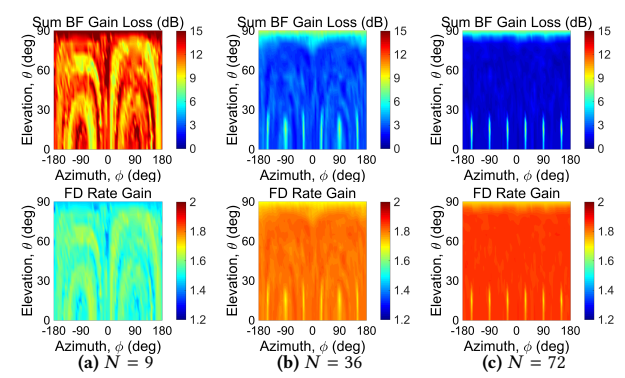


Figure 13: Spatial distributions of the sum TxBF and RxBF gain loss (top row), and the FD rate gain in the BS-User case when the user is in different spatial directions from the FD BS (bottom row), with  $N \in \{9, 36, 72\}$ ,  $P_t = 30 \, \text{dBm}$ , and  $\gamma_{bu} = \gamma_{ub} = 0 \, \text{dB}$ .

under the iterative FD TxBF and RxBF with varying  $P_t$  and link SNR values. The results show that although the FD phased array experiences TxBF and RxBF gain losses to achieve  $\gamma_{bb}(f_k) \leq 1$ ,  $\forall k$ , an FD rate gain of at least  $1.53\times$  can be achieved with  $N\geq 36$  in all SNR regimes. Also, the FD rate gain improves with increased values of both N and the link SNR. Moreover, when the number of antennas is large, further increasing N introduces only marginal FD rate gain since the SI power is already canceled to below the noise floor with a smaller value of N (see Section 5).

To compare the performance of the iterative and optimal FD TxBF and RxBF, Table 1 summarizes the average ratio between the FD rate gains achieved by the iterative (with  $\widetilde{g_t}$  and  $\widetilde{g_r}$ ) and optimal (with  $g^*$ ) FD TxBF and RxBF. The results show that the FD rate gains achieved under  $\widetilde{g_t}$  and  $\widetilde{g_r}$  are very close to that achieved under  $g^*$  (i.e., the average ratio is at least 89%) in all considered scenarios. **BS-User Case with Spatially Distributed Users**. To evaluate the FD rate gain, we consider spatially distributed users in the directions of  $\phi \in [-180^\circ, 180^\circ]$  and  $\theta \in [0^\circ, 90^\circ]$  with respect to the BS. The BS applies the iterative FD TxBF and RxBF with the desired Tx and Rx beam-pointing directions equal to the user direction. We consider the low SNR regime with  $N \in \{9, 36, 72\}$  and  $P_t = 30$  dBm (see Section 5). Fig. 13 plots the spatial distribution of the sum TxBF and RxBF gain loss for achieving  $\gamma_{bb}(f_k) \leq 1$ ,  $\forall k$ , and the resulting FD rate gain with low UL and DL SNR values of 0 dB.

The results show that the sum TxBF and RxBF gain loss varies across all spatial directions, since the total SI power depends on both the array geometry and the beam-pointing directions. The SI power is the strongest in the array broadside (z-axis) and in the direction of adjacent antennas close to the array xy-plane (e.g.,  $\phi=\pm90^\circ$  for N=9 and  $\phi=\pm30/90/150^\circ$  for  $N\in\{36,72\}$ , with very small values of  $\theta$ ). Yet, the iterative FD TxBF and RxBF is still able to achieve  $\gamma_{bb}(f_k)\leq 1$  under  $P_t=30$  dBm with maximum sum TxBF and RxBF gain losses of 9.7/8.6 dB for N=36/72. Overall, the FD rate gains are at least 1.33/1.66/1.68× for N=9/36/72, and when the user is not in the direction of the strongest SI power, the FD rate gains can be increased to 1.68/1.83/1.87× for N=9/36/72. Note that higher link SNR values also increase FD rate gain at the same sum TxBF and RxBF gain loss.

**Efficiency of the Iterative Algorithm.** We compare the performance of the iterative FD TxBF and RxBF to the optimal TxBF

Table 2: Runtime improvements of the iterative algorithm over directly solving the non-convex (Opt-TxRx).

N	9	18	27	36	45	54	63	72
Impr.	0.99×	1.72×	2.41×	2.12×	2.70×	3.18×	5.51×	6.00×
Sum Beamforming Gain Loss (dB)  0 0 0	$P_{\rm t} = 30  {\rm d}$ $P_{\rm t} = 20  {\rm d}$ $P_{\rm t} = 10  {\rm d}$	IBm IBm IBm 40 50 (MHz)	1.8 4 1.6 9 1.4 1.2 L 2 1.2 L	$P_{t} = 30$ or $P_{t} = 20$ or $P_{t} = 10$	IBm IBm IBm 40 50	8.1 A Rate Gain 1.2 L P R R R R R R R R R R R R R R R R R R		0 dBm 0 dBm 0 dBm 30 40 50

Figure 14: Sum TxBF and RxBF gain loss, and FD rate gains in the BS-User and BS-BS cases with N=8 and varying desired RF SIC bandwidth,  $B\in\{10,\ldots,50\}\,\mathrm{MHz}$ , and  $P_{\mathbf{t}}\in\{10,20,30\}\,\mathrm{dBm}$ .

and RxBF in terms of the time consumed to obtain the Tx and Rx beamformers. We perform 100 runs of solving (Opt-TxRx) and of the iterative algorithm in all considered values of N and  $P_t$ , and measure the average running times. Table 2 summarizes the improvements in the average running time of the iterative TxBF and RxBF over the optimal TxBF and RxBF. The results show that with N = 9, both FD TxBF and RxBF have similar running times. However, as N increases, the iterative TxBF and RxBF outperforms the optimal TxBF and RxBF due to the non-convexity of (Opt-TxRx). **Effect of the Bandwidth,** B. Lastly, we evaluate the effects of the desired RF SIC bandwidth, B, on the FD TxBF and RxBF using the measurements of the 8-element rectangular array with circulators (recall that the Argos dataset is only with B = 20 MHz). We consider the iterative FD TxBF and RxBF with  $B \in \{10, ..., 50\}$  MHz and  $P_t \in \{10, 20, 30\}$  dBm. Fig. 14 plots the sum TxBF and RxBF gain loss and the corresponding FD rate gain in both the BS-User and BS-BS cases. The results show that, even with only 8 elements, an FD phased array can achieve  $\gamma_{bb}(f_k) \leq 1, \forall k$ , for up to B =50 MHz at  $P_t = 10$  dBm, where the sum TxBF and RxBF gain loss is at most 8.5 dB (TxBF/RxBF gain loss of 4.4 dB/4.1 dB). The sum TxBF and RxBF gain loss increases to 12.3 dB with  $P_t = 20$  dBm. However, although higher TxBF and RxBF gain losses are required in scenarios with increased P<sub>t</sub> and B, an 8-element FD phased array is able to achieve FD rate gains of at least 1.47/1.42/1.36× under  $P_t = 10/20/30$  dBm, with bandwidth of up to B = 50 MHz.

#### 8 CONCLUSIONS

In this paper, we considered FD phased arrays in which TxBF and RxBF are repurposed to achieve wideband RF SIC. We formulated optimization problems to obtain the maximum FD TxBF and RxBF gains and developed an iterative algorithm to efficiently solve the optimization problems. Using measurements and datasets, we extensively evaluated the performance of the FD phased array and the resulting FD rate gains in various network settings. Future directions include: (i) system design and implementation of a large-scale FD phased array based on our previous work [13], and its integration in the city-scale COSMOS testbed [8, 27], and (ii) experimental evaluation of the FD TxBF and RxBF approach.

#### **ACKNOWLEDGMENTS**

This work was supported in part by NSF grants ECCS-1547406, CNS-1650685, and CNS-1827923.

#### REFERENCES

- $[1]\ \ 2016.\ Argos\ full-duplex\ channel\ measurement\ dataset.\ http://data.argos.rice.edu/.$
- [2] Ehsan Aryafar and Alireza Keshavarz-Haddad. 2018. PAFD: Phased array fullduplex. In Proc. IEEE INFOCOM'18.
- [3] Ehsan Aryafar, Mohammad Amir Khojastepour, Karthikeyan Sundaresan, Sampath Rangarajan, and Mung Chiang. 2012. MIDU: Enabling MIMO full duplex. In Proc. ACM MobiCom'12.
- [4] Dimitri P Bertsekas and John N Tsitsiklis. 1989. Convergence rate and termination of asynchronous iterative algorithms. In Proc. ACM ICS'89.
- [5] Dinesh Bharadia and Sachin Katti. 2014. Full duplex MIMO radios. In Proc. USENIX NSDI'14.
- [6] Dinesh Bharadia, Emily McMilin, and Sachin Katti. 2013. Full duplex radios. In Proc. ACM SIGCOMM'13.
- [7] Lu Chen, Fei Wu, Jiaqi Xu, Kannan Srinivasan, and Ness Shroff. 2017. BiPass: Enabling end-to-end full duplex. In Proc. ACM MobiCom'17.
- [8] Tingjun Chen, Mahmood Baraani Dastjerdi, Jin Zhou, Harish Krishnaswamy, and Gil Zussman. 2018. Open-access full-duplex wireless in the ORBIT testbed. arXiv preprint arXiv:1801.03069 (2018).
- [9] Tingjun Chen, Mahmood Baraani Dastjerdi, Jin Zhou, Harish Krishnaswamy, and Gil Zussman. 2019. Wideband full-duplex wireless via frequency-domain equalization: Design and experimentation. In Proc. ACM MobiCom'19 (to appear).
- [10] Tingjun Chen, Jelena Diakonikolas, Javad Ghaderi, and Gil Zussman. 2018. Hybrid scheduling in heterogeneous half-and full-duplex wireless networks. In Proc. IEEE INFOCOM'18.
- [11] MinKeun Chung, Min Soo Sim, Jaeweon Kim, Dong Ku Kim, and Chan-Byoung Chae. 2015. Prototyping real-time full duplex radios. *IEEE Commun. Mag.* 53, 9 (2015), 56–63.
- [12] A Balanis Constantine. 2005. Antenna theory: Analysis and design, third edition. John Wiley & Sons.
- [13] Mahmood Baraani Dastjerdi, Negar Reiskarimian, Tingjun Chen, Gil Zussman, and Harish Krishnaswamy. 2018. Full duplex circulator-receiver phased array employing self-interference cancellation via beamforming. In Proc. IEEE RFIC'18.
- [14] Melissa Duarte, Chris Dick, and Ashutosh Sabharwal. 2012. Experiment-driven characterization of full-duplex wireless systems. *IEEE Trans. Wireless Commun.* 11, 12 (2012), 4296–4307.
- [15] Melissa Duarte, Ashutosh Sabharwal, Vaneet Aggarwal, Rittwik Jana, KK Ramakrishnan, Christopher W Rice, and NK Shankaranarayanan. 2014. Design and characterization of a full-duplex multiantenna system for WiFi networks. IEEE Trans. Veh. Technol. 63, 3 (2014), 1160–1177.
- [16] Evan Everett, Clayton Shepard, Lin Zhong, and Ashutosh Sabharwal. 2016. Softnull: Many-antenna full-duplex wireless via digital beamforming. *IEEE Trans. Wireless Commun.* 15, 12 (2016), 8077–8092.
- [17] Harish Krishnaswamy and Gil Zussman. 2016. 1 Chip 2x the bandwidth. IEEE Spectrum 53, 7 (2016), 38–54.
- [18] Yan Liu, Yuan Shen, Dongning Guo, and Moe Z Win. 2018. Network localization and synchronization using full-duplex radios. *IEEE Trans. Signal Process.* 66, 3 (2018), 714–728.
- [19] Jelena Marasevic and Gil Zussman. 2016. On the capacity regions of singlechannel and multi-channel full-duplex links. In Proc. ACM MobiHoc'16.
- [20] Zhenzhi Qian, Fei Wu, Zizhan Zheng, Kannan Srinivasan, and Ness B Shroff. 2017. Concurrent channel probing and data transmission in full-duplex MIMO systems. In Proc. ACM MobiHoc'17.
- [21] Taneli Riihonen, Arun Balakrishnan, Katsuyuki Haneda, Shurjeel Wyne, Stefan Werner, and Risto Wichman. 2011. Optimal eigenbeamforming for suppressing self-interference in full-duplex MIMO relays. In Proc. IEEE CISS'11.
- [22] Ashutosh Sabharwal, Philip Schniter, Dongning Guo, Daniel W Bliss, Sampath Rangarajan, and Risto Wichman. 2014. In-band full-duplex wireless: Challenges and opportunities. IEEE J. Sel. Areas Commun. 32, 9 (2014), 1637–1652.
- [23] Clayton Shepard, Hang Yu, Narendra Anand, Erran Li, Thomas Marzetta, Richard Yang, and Lin Zhong. 2012. Argos: Practical many-antenna base stations. In Proc. ACM MobiCom'12.
- [24] Guobao Sun, Fan Wu, Xiaofeng Gao, and Guihai Chen. 2012. PHED: Prehandshaking neighbor discovery protocols in full duplex wireless ad hoc networks. In Proc. IEEE GLOBECOM'12.
- [25] Barry D Van Veen and Kevin M Buckley. 1988. Beamforming: A versatile approach to spatial filtering. IEEE ASSP Mag. 5, 2 (1988), 4–24.
- [26] Yang Yang and Ness B Shroff. 2015. Scheduling in wireless networks with full-duplex cut-through transmission. In Proc. IEEE INFOCOM'15.
- [27] Jiakai Yu, Tingjun Chen, Craig Gutterman, Shengxiang Zhu, Gil Zussman, Ivan Seskar, and Dan Kilper. 2019. COSMOS: Optical architecture and prototyping. In Proc. OSA OFC'19.
- [28] Jin Zhou, Negar Reiskarimian, Jelena Diakonikolas, Tolga Dinc, Tingjun Chen, Gil Zussman, and Harish Krishnaswamy. 2017. Integrated full duplex radios. IEEE Communn. Mag. 55, 4 (2017), 142–151.